doi:10.1016/j.jmb.2008.07.062 J. Mol. Biol. (2008) 383, 347–357

JMB

Available online at www.sciencedirect.com

ScienceDirect

ELSEVIER

Structural and Kinetic Analysis of Pyrrolidine-Based Inhibitors of the Drug-Resistant Ile84Val Mutant of HIV-1 Protease

Jark Böttcher†, Andreas Blum†, Andreas Heine, Wibke E. Diederich and Gerhard Klebe*

Institut für Pharmazeutische Chemie, Philipps-Universität Marburg, Marbacher Weg 6, 35032 Marburg, Germany

Received 12 March 2008; received in revised form 22 July 2008; accepted 24 July 2008
Available online 29 July 2008

Human immunodeficiency virus (HIV) protease is a well-established drug target in HIV chemotherapy. However, continuously increasing resistance towards approved drugs inevitably requires the development of new inhibitors preferably showing no susceptibility against resistant HIV protease strains. Recently, symmetric pyrrolidine-3,4-bis-*N*-benzyl-sulfonamides have been developed as a new class of HIV-1 protease inhibitors. The most promising candidate exhibited a K_i of 74 nM towards a wild-type protease. Herein, we report the influence of the active-site mutations Ile50Val and Ile84Val on these inhibitors by structural and kinetic analysis. Although the Ile50Val mutation leads to a significant decrease in affinity for all compounds in this series, they retain or even show increased affinity towards the important Ile84Val mutation. By detailed analysis of the crystal structures of two representatives in complex with wild-type and mutant proteases, we were able to elucidate the structural basis of this phenomenon.

Keywords: HIV protease; drug resistance; pyrrolidine-based inhibitors; kinetic analysis; crystallography

Edited by R. Huber

Introduction

Human immunodeficiency virus (HIV) protease is a well-established target for the development of antiviral therapeutics.[1] The protease processes the *gag*- and *gag-pol*-encoded polyproteins into functional enzymes that are essential for the viral replication.[2] Inhibition of the viral protease leads to immature noninfectious virions.[3] Currently, nine HIV protease inhibitors (PIs) are approved by the U.S. Food and Drug Administration.[4] The highly active antiretroviral therapy, which combines protease and reverse transcriptase inhibitors, not only significantly prolongs but also improves the quality of the patient's life.[5,6] However, an entire remedy of the infection still remains an unaccomplished goal. Moreover, although most of the inhibitors initially exhibit a strong inhibitory effect, this efficacy decreases over time due to the continuously new formation of drug-resistant virus variants.

The relatively low fidelity of the viral reverse transcriptase and the fast replication rate are the main driving factors for the high mutation rate of the HIV. It has been estimated that up to 10^5 point mutations occur daily within the viral population of an infected individual.[7] Due to high mutation rates, there are several nonidentical genomes termed viral quasispecies, hence making it difficult to define one wild-type protease as reference point.[8] The following studies were performed using a clone of the BH10 isolate. Mutations in the binding pocket as well as in distal sites of the HIV protease affect inhibitor and substrate binding by altering the number and strength of subsite interactions. Since the applied inhibitors effectively inhibit wild-type proteases and limit wild-type duplication, they also provide a selective advantage to those HIV variants with reduced susceptibility. The occurrence of multi-drug-resistant HIV variants diminishing the efficacy of all PIs in clinical use hampers an effective antiviral treatment of patients infected by these variants. Under selective drug pressure, mutations have been

*Corresponding author. E-mail address: klebe@mailer.uni-marburg.de.

† J. B. and A. B. contributed equally to this work.

Abbreviations used: HIV, human immunodeficiency virus; PI, protease inhibitor; PDB, Protein Data Bank; DMSO, dimethyl sulfoxide.

0022-2836/$ - see front matter © 2008 Published by Elsevier Ltd.

proven to occur nearly in one-half of the HIV-1 protease amino acid positions.[9] The mutations can generally be classified into major and minor ones.[10] Major mutations are initially selected by drug treatment and mainly occur at residues forming interactions upon drug binding. Minor mutations consecutively improve the replicative fitness of virus variants carrying major mutations.

The high adaptability of the virus demands a continuous and persistent search for new inhibitors. Novel inhibitors should exhibit a different mutation profile compared to that of the marketed drugs to circumvent the development of cross-resistance. Most of the currently approved inhibitors are transition-state mimics targeting the catalytic aspartates 25A and 25B via a secondary hydroxyl group. As an alternative skeleton, cyclic amines have been proposed as novel anchoring groups.[11] Very recently, we have described the design and synthesis of C_2-symmetric 3,4-disubstituted pyrrolidines as a new class of HIV-1 PIs. The co-crystal structures of six derivatives were determined in complex with wild-type HIV-1 protease {compound [Protein Data Bank (PDB) ID]: **1** (2PQZ), **3** (2QNP), **6** (2QNQ), **8** (2PWC), **9** (2PWR), **10** (2QNN); Table 2} and further utilized within a structure-guided optimization process.[12] These crystal structures revealed a conserved binding mode for all investigated derivatives, schematically represented in Fig. 1: The endocyclic amino function addresses the catalytic dyad and a unique flap interaction pattern is observed. Only one sulfonyl group of the C_2-symmetric inhibitor is involved in two hydrogen bonds to the backbone NHs of Ile50A and Ile50B each formed by one of the sulfonyl oxygen atoms. The second sulfonyl group remains uncoordinated and establishes no polar contacts. This leads to an overall slightly asymmetric binding mode of the C_2-symmetric inhibitors. However, each symmetry-related subpocket is occupied by the corresponding symmetry-related substituent of the inhibitor. For the wildtype protease, the co-crystal

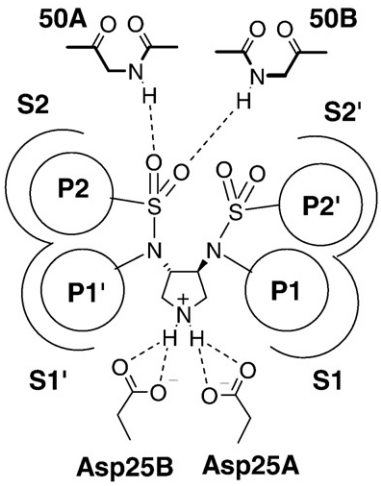

Fig. 1. Schematic representation of the conserved binding mode of the pyrrolidine-3,4-bis-*N*-benzyl-sulfonamides. Hydrogen bonds are indicated by broken lines and main-chain bonds are denoted by bold lines.

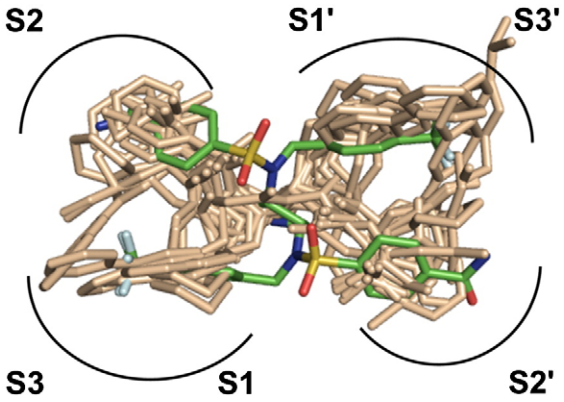

Fig. 2. Superposition of the final lead structure (compound **10**) with the co-crystal structures of all approved HIV PIs, based on crystal structures with the wildtype. Compound **10** is shown in green, color coded by atom type, whereas the ligand geometries of the approved PIs are displayed in wheat.

structure of the most potent derivative (compound **10**)[12] is shown together with the co-crystal structures of all currently approved HIV PIs in Fig. 2 [inhibitor (PDB ID): ritonavir (1HXW),[13] atazanavir (2AQU),[14] darunavir (1T3R),[15] amprenavir (1HPV),[16] indinavir (1HSG),[17] nelfinavir (1OHR),[18] saquinavir (1HXB),[19] lopinavir (2O4S),[20] and tipranavir (2O4P)[20]]. This comparison reveals a completely different mode in targeting the protease's subsites by this new class of inhibitors: Whereas the approved inhibitors bind to the subsites successively from S3 to S3′, the pyrrolidine-based inhibitors occupy the S1–S3/S2′ and the S1′–S3′/S2 pockets via the two substituents at the pyrrolidine ring, respectively. This leads to a unique binding mode in the active site, particularly at the borders of the S1/S2′ and the S1′/S2 pockets, composed of the amino acids Ile50 and Ile84 of chain A and B. Both residues are referred to as major mutations. Whereas the Ile84Val mutation in HIV-1 protease is associated with resistance to all approved inhibitors, the Ile50Val mutation is mainly linked to the resistance against amprenavir.[21]

Due to their importance and the remarkable differences in binding of the pyrrolidine-based inhibitors, particularly in the contact area next to Ile50 and Ile84, we selected these two mutations for further investigations. Both mutations have already been studied extensively by kinetic measurements,[22,23] structural biology,[24,25] isothermal calorimetry,[26,27] and computational methods.[28] These studies attribute the reduced affinity with respect to the Ile84Val mutant primarily to the loss of van der Waals contacts with the P1/P1′ moieties of the inhibitors. The sensitivity of amprenavir towards the Ile50Val mutation is attributed to strong interactions of the C^{δ} of Ile50A with the P2′ residue of the inhibitor.[26]

Encouraged by the deviating and up to now unique mode in which the C_2-symmetric pyrrolidine-based inhibitors bind to the protease's subsites, we investigated their potential against these drug-resistant mutations. The two active-site mutants Ile50Val and

Ile84Val were generated by site-directed mutagenesis. Followed by kinetic studies, two representatives (compounds **8** and **9**) were crystallized in complex with the wild-type and the two corresponding mutant proteases. Throughout this article, the wild-type protease (BH10 isolate) is referred to as PR_{WT} and the mutant proteases are referred to as PR_{I50V} and PR_{I84V}.

Results

Kinetic characterization

In order to estimate the consequences of the point mutations to putative natural substrates, the kinetic parameters of PR_{WT}, PR_{I50V}, and PR_{I84V} were determined in a fluorescence-based assay (Table 1) using four different commercially available substrates. The four fluorescence substrates were purchased from Bachem (substrates A and B) and Sigma-Aldrich (substrates C and D). PR_{I50V} and PR_{I84V} exhibited a significantly reduced K_m to all studied substrates compared to PR_{WT}. For PR_{I50V}, the affinity towards the substrates is reduced 10-fold, whereas for PR_{I84V}, an affinity reduction by a factor of 5 was determined. The reduced catalytic efficiency (k_{cat}/K_m) is driven by this loss in affinity of the mutant proteases towards these substrates.

The affinities of the pyrrolidine-based inhibitors were determined towards the protease variants using substrate A, and the results are summarized in Table 2. In the case of the Ile50Val mutation, on average, a decrease in affinity of the pyrrolidine-based inhibitors by a factor of 5 is observed. This overall decrease in affinity seems therefore to occur as a general phenomenon of this class of compounds and not as a result of a special substitution pattern. In contrast, the pyrrolidine-based inhibitors exhibit an equal or even improved affinity towards the Ile84Val mutant: Pyrrolidine **1** exhibits a twofold increase in affinity. Compounds with only one additional hydrophobic substituent at the P1/P1′ aromatic rings (compounds **2**, **3**, and **4**) at least retain their affinity, whereas all other derivatives carrying additional polar or hydrophobic substituents at the P2/P2′ moieties exhibit significantly improved potency. Particularly for the amide-substituted derivatives (compounds **9** and **10**), an up to sevenfold increase in affinity towards this drug-resistant point mutant is observed. To investigate the contrasting behavior of the inhibitors towards the single point mutants PR_{I50V} and PR_{I84V}, we determined the co-crystal structures of two derivatives in complex with the mutant proteases. Due to the largest relative difference in affinity towards the mutants, along with good potency, compounds **8** and **9** were selected, possessing deviating P2/P2′ substituents.

Structural analysis

The amino (**8**) and carboxamido (**9**) derivatives were crystallized in complex with the PR_{I50V} and PR_{I84V} variants. The crystallographic data and refinement statistics of the four structures are listed in Table 3. All co-crystal structures discussed within this study crystallized, with identical packing, in the space group $P2_12_12$ with very similar lattice constants. Therefore, an influence of crystal packing on the observed differences can be neglected. In the space group $P2_12_12$, the asymmetric unit contains the HIV-1 protease with two symmetry-independent chains labeled as 1A to 99A and 1B to 99B, respectively. The collected data sets have comparable quality with resolutions between 1.58 and 1.92 Å. In all cases, the ligand geometries were clearly visible in the F_o-F_c omit map at a σ level of 3.0 (Fig. 3) and could be refined as one single conformer. All structures were determined by molecular replacement and consecutively refined following the same protocol.

Crystal structures of compound 8

The crystal structures of the amino derivative (compound **8**) in complex with the HIV protease variants were determined with a resolution of 1.58 Å (PR_{I50V}) and 1.92 Å (PR_{I84V}), respectively. Both complexes exhibit a high level of similarity to the corresponding wild-type complex (determined at a resolution of 1.78 Å) studied previously.[12] This similarity is reflected by the root-mean-square deviation (rmsd) between the C^α atoms of 0.12 Å for PR_{I50V} and 0.18 Å for PR_{I84V} compared to the PR_{WT} complex. Using the C^α-based alignment, the ligand geometries also show a high level of similarity with an rmsd of 0.19 Å for the PR_{I50V} and 0.28 Å for the PR_{I84V} in comparison to the PR_{WT} ligand coordinates (Fig. 4a). The overall binding mode is conserved and schematically represented in Fig. 5a; the distances of polar contacts are given in

Table 1. Kinetic characterization of PR_{WT}, PR_{I50V}, and PR_{I84V} with fluorogenic substrates

Anthranilyl-HIV protease substrate	WT		PR_{I50V} (/WT)		PR_{I84V} (/WT)	
	K_m (μM)	k_{cat}/K_m ($\mu M^{-1}\ s^{-1}$)	K_m (μM)	k_{cat}/K_m ($\mu M^{-1}\ s^{-1}$)	K_m (μM)	k_{cat}/K_m ($\mu M^{-1}\ s^{-1}$)
A	14.6±0.9	0.41±0.07	139±9 (10)	0.013±0.003 (0.03)	70.6±1.3 (5)	0.057±0.003 (0.03)
B	22.7±2.6	0.36±0.13	158±24 (7)	0.048±0.023 (0.1)	72.0±7.2 (3)	0.090±0.026 (0.1)
C	9.7±0.6	1.87±0.34	117±5 (12)	0.21±0.025 (0.1)	51.3±2.6 (5)	0.46±0.056 (0.1)
D	5.2±0.4	1.66±0.36	54.9±1.9 (11)	0.21±0.026 (0.1)	27.7±2.1 (5)	0.41±0.08 (0.1)

Values in parentheses refer to the relative change compared to the wild-type protease.

Table 2. K_i values of the inhibitors towards the wild-type and mutant HIV proteases

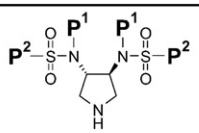

	P^2	P^1	PR_{WT} K_i [μM]	PR_{I50V} K_i [μM]	PR_{I84V} K_i [μM]	K_i I50V/WT	K_i I84V/WT
1		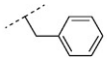	2.2	10.9	1.1	5	0.5
2		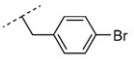	0.46	2.6	0.55	6	1.2
3		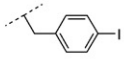	0.39	1.4	0.33	4	0.8
4		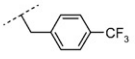	0.80	3.0	0.50	4	0.6
5		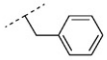	0.67	2.1	0.46	3	0.7
6		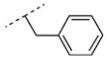	0.77	2.6	0.48	3	0.6
7	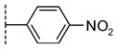	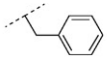	1.7	8.0	0.92	5	0.5
8	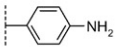	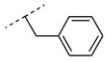	0.27	1.0	0.128	4	0.5
9	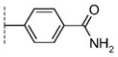	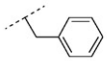	0.26	1.4	0.036	5	0.1
10	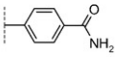	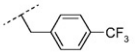	0.07	0.26	0.012	4	0.2

Table 4. The pivotal nitrogen of the pyrrolidine core structure interacts with the catalytic dyad. In the case of the wild-type complex, the nitrogen atom is in close contact with the carboxylic oxygen atoms of Asp25A and Asp25B. This important interaction is conserved for the mutant proteases. The flap interactions formed via hydrogen bonds of the sulfonyl oxygens to the main-chain NH of Ile50A and Ile50B or Val50A and Val50B are comparable in all complexes. The inhibitor's benzyl moieties occupy the S1 and S1′ pockets whereas the *p*-amino-phenyl sulfonamide groups bind in the S2 and S2′ pockets. The amino substituents form a hydrogen-bond network, which, due to the asymmetric binding mode, differs in S2 and S2′. The observed polar interactions in S2 are highly conserved: The amino group hydrogen bonds to the main-chain carbonyl oxygen of Asp30B and, mediated via a water molecule, to the corresponding side-chain carboxyl oxygen atom. In the S2′ pocket, differences are noticed: The water-mediated interaction to the carboxyl function of Asp29A is only observed in PR_{WT} and PR_{I50V}, whereas the H-bond to the side chain of Asp30A is conserved in all complexes. In PR_{WT} and PR_{I50V}, the C^{δ} atoms of Ile84A and Ile84B are in close van der Waals contact to the benzylic methylene groups of the ligand (PR_{WT}, 3.5/3.3 Å; PR_{I50V}, 3.6/3.4 Å), compared to C^{γ} of the corresponding Val84A and Val84B in PR_{I84V} (3.8/4.0 Å). The burial of the ligand surface varies slightly between 95% and 96%, exhibiting the highest value in the PR_{WT} complex.

The most pronounced differences are observed in the PR_{I84V} complex: The Ile84Val exchange at the border of the S1/S2′ pockets enlarges the binding site, and the newly created additional space is filled by a water molecule (O3083, Fig. 5b). This water mediates polar interactions between one oxygen atom of the sulfonyl group of compound **8** and the main-chain carbonyl of Val82A and the side chain of

Table 3. Crystallographic data for the complexes of the amino derivative (compound **8**) and the carboxamido derivative (compound **9**)

	8		**9**	
	PR_{I50V}	PR_{I84V}	PR_{I50V}	PR_{I84V}
Resolution (Å)	25–1.58	25–1.92	30–1.80	30–1.81
Space group	$P2_12_12$	$P2_12_12$	$P2_12_12$	$P2_12_12$
Cell dimensions (Å)				
a	57.9	57.3	57.2	57.4
b	86.0	85.7	85.5	85.7
c	46.3	46.6	46.7	46.6
Highest-resolution shell (Å)	1.61–1.58	1.95–1.92	1.83–1.80	1.84–1.81
No. of measured reflections	141,102	76,478	89,944	75,858
No. of independent reflections	31,985	17,926	20,882	21,217
Completeness (%)	99.1 (90.6)	98.6 (97.0)	95.5 (100)	97.8 (100)
I/σ	13.5 (2.5)	15.8 (3.2)	18.8 (3.1)	16.2 (2.6)
R_{sym} (%)	9.0 (37.5)	9.1 (46.3)	7.3 (49.1)	7.0 (42.2)
Resolution in refinement (Å)	10–1.58	10–1.92	10–1.80	10–1.81
R_{cryst} ($F>4\ \sigma\ F_o$; F_o) (%)	17.0; 19.8	17.8; 20.1	17.7; 19.3	18.1; 20.4
R_{free} ($F>4\ \sigma\ F_o$; F_o) (%)	20.7; 24.5	23.0; 26.4	23.3; 25.3	23.8; 26.0
Mean *B*-factor (Å^2) (peptide chain A; peptide chain B)	15.2; 13.5	27.3; 24.9	31.9; 28.4	23.3; 21.1
Main chain (Å^2)	12.3; 11.2	24.8; 22.5	28.3; 25.8	20.7; 19.0
Side chains (Å^2)	18.2; 15.9	30.2; 27.5	35.9; 31.2	26.4; 23.5
Ligand (Å^2)	20.3	27.1	25.3	20.7
Water molecules (Å^2)	24.8	31.0	35.4	27.9
Ramachandran plot (%)				
Most favored geometry	96.8	95.6	97.5	94.9
Additionally allowed	3.2	4.4	2.5	5.1
rmsd bonds (Å)	0.007	0.005	0.006	0.006
rmsd angles (°)	2.0	1.9	2.0	1.9

Values in parentheses refer to the highest-resolution shell.

Thr80A. The binding pockets of the three structures were consecutively analyzed with a water probe using the program GRID to evaluate whether the position of the additional water is energetically favorable. In Fig. 6c, the GRID interaction fields for the PR_{I84V} binding pocket are displayed. A contour is observed at the position of the additionally enclosed water molecule, together with an area next to the catalytic Asp25A and Asp25B and at the far end of S2 and S2′ and near Gly27A and Gly27B, which are part of the peptide recognition motif. The positions of the experimentally observed water molecules are in good agreement with the calculated fields. In the case of the PR_{WT} (Fig. 6a) and the PR_{I50V} (Fig. 6b) complexes, similar observations are made except for the GRID interaction field near Thr80A and Val82A.

Crystal structures of compound 9

The crystal structures of the carboxamido derivative (compound **9**) were determined with a resolution of 1.80 Å (PR_{I50V}) and 1.81 Å (PR_{I84V})

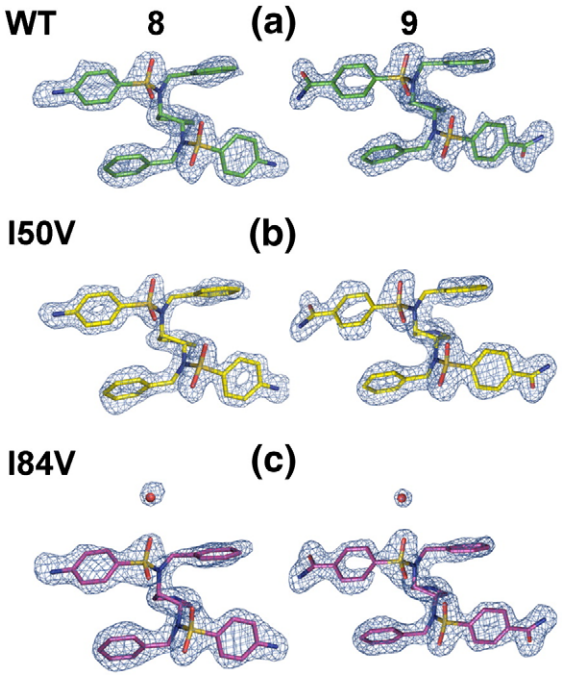

Fig. 3. Ligand geometries of compounds **8** and **9** color coded by atom type in the co-crystal structures with PR_{WT}: (a) green, PR_{I50V}: (b) yellow, and PR_{I84V}: (c) magenta. The $F_o - F_c$ omit map for the ligand and the water in the case of (c) is displayed at a σ level of 3.0 as blue mesh.

(Table 3). As for compound **8**, the overall binding of compound **9** is conserved compared to the wild-type counterpart (1.50 Å) described previously.[12] Compared to the PR_{WT} structure, the C^{α} rmsd of PR_{I50V} and PR_{I84V} is 0.23 and 0.24 Å, respectively. The corresponding rmsd for the ligand atoms using this alignment is 0.19 Å for PR_{I50V} and 0.28 Å

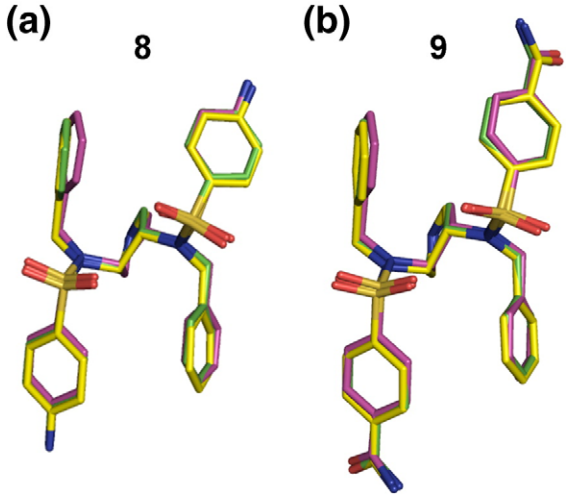

Fig. 4. Ligand geometries of the C^{α} superposition of the co-crystal structures of compounds **8** (a) and **9** (b) in complex with PR_{WT} (green), PR_{I50V} (yellow), and PR_{I84V} (magenta), color coded by atom type.

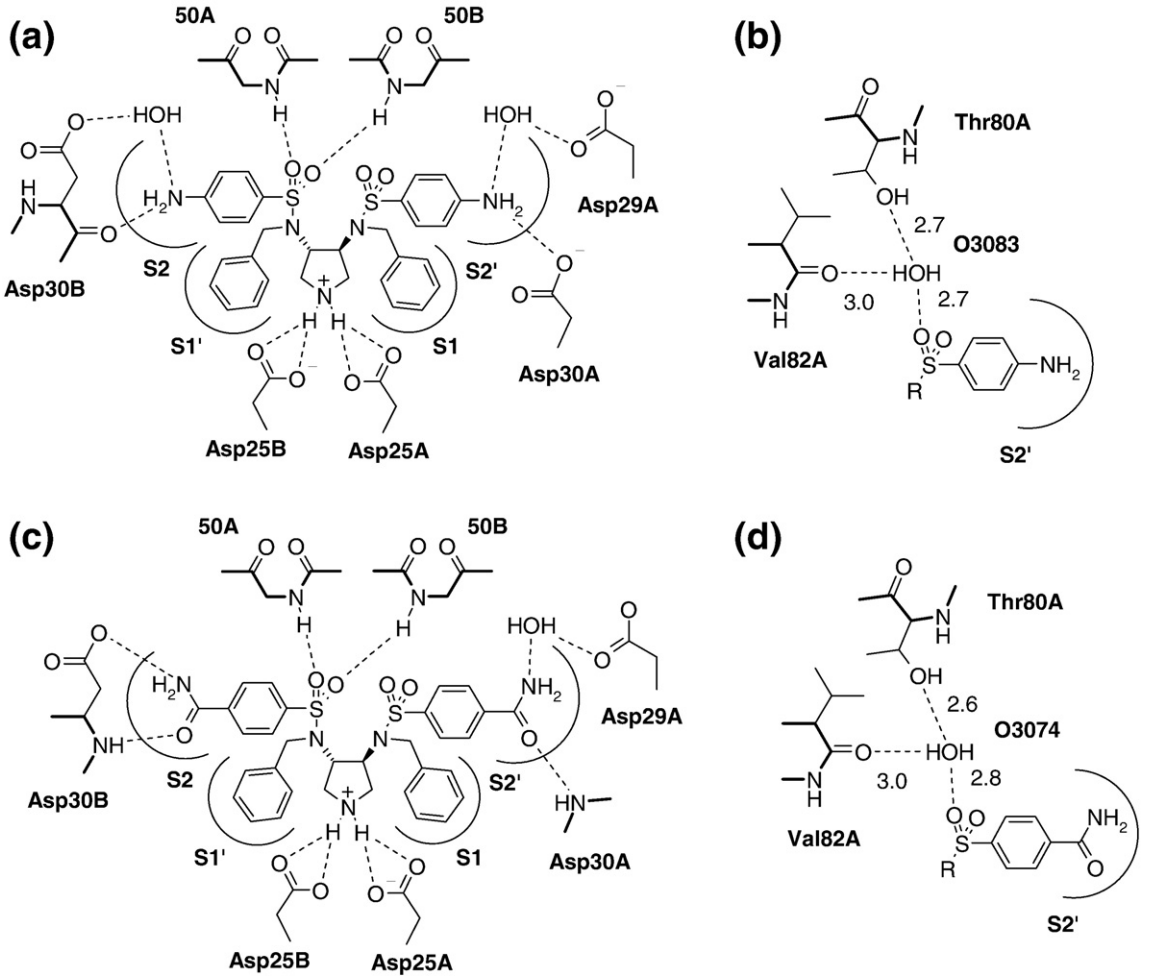

Fig. 5. Schematic representation of the binding modes of compounds **8** (a) and **9** (c) observed in the crystal structures in complex with PR_{WT}, PR_{I50V}, and PR_{I84V}. Additional hydrogen-bond network of water O3083 in the case of compound **8** (b) and water O3074 in the case of compound **9** (d) in complex with PR_{I84V}. Hydrogen bonds are indicated by broken lines and main-chain bonds are denoted by bold lines.

for PR_{I84V} (Fig. 4b). The same subsite occupancy is observed in all complexes and is schematically represented in Fig. 5c. The hydrogen bond network established by the inhibitor is conserved, and the polar contact distances are given in Table 5. The pivotal nitrogen is in close polar contact to the carboxylate oxygens of Asp25A and Asp25B, while the flap only interacts with the oxygen atoms of one sulfonyl group forming hydrogen bonds to the main-chain NHs of amino acid residues 50A and 50B. In S2, direct interactions of the carboxamido oxygen to the main-chain NH of Asp30B and of the carboxamido nitrogen to the corresponding Asp30B side chain are observed in all complexes. The water-mediated interaction to the side chain of Asp29A and the direct interaction to the backbone NH of Asp30A in S2′ exhibit a high level of similarity. The C^{δ} atoms of Ile84A and Ile84B are in close contact to the benzylic methylene groups of the ligand (PR_{WT}, 3.3/3.3 Å; PR_{I50V}, 3.5/3.6 Å). In PR_{I84V}, the C^{γ} atoms of Val84A and Val84B only show van der Waals contacts of 3.8 and 4.1 Å. The burial of the ligand surface within the binding pocket sums up to 95% in the case of PR_{I50V} and to 96% in the case of PR_{WT} and PR_{I84V}.

An intercalation of a water molecule (O3074) is observed in PR_{I84V} and results in additional polar protein–ligand interactions. The water molecule establishes hydrogen bonds to the backbone carbonyl of Val82A, to the side chain of Thr80A, and to one ligand sulfonyl oxygen atom (Fig. 5d). The binding pockets were analyzed with the program GRID. The resulting interaction fields of a water probe for PR_{I84V} are displayed in Fig. 6f.

Table 4. Polar contacts of ligand **8** observed in the co-crystal structures with the different HIV protease variants

	PR_{WT} (Å)	PR_{I50V} (Å)	PR_{I84V} (Å)
D25 O^{δ}	2.6–3.0	2.7–3.0	2.7–3.0
I/V50A N	3.1	3.0	3.2
I/V50B N	3.7	3.8	3.7
D29A O^{δ}/H_2O	3.2/2.9	3.3/2.8	—
D30A O^{δ}	2.7	2.7	2.7
D30B O^{δ}/H_2O	2.8/2.7	2.9/2.7	2.8/2.8
D30B O	3.2	3.1	3.1

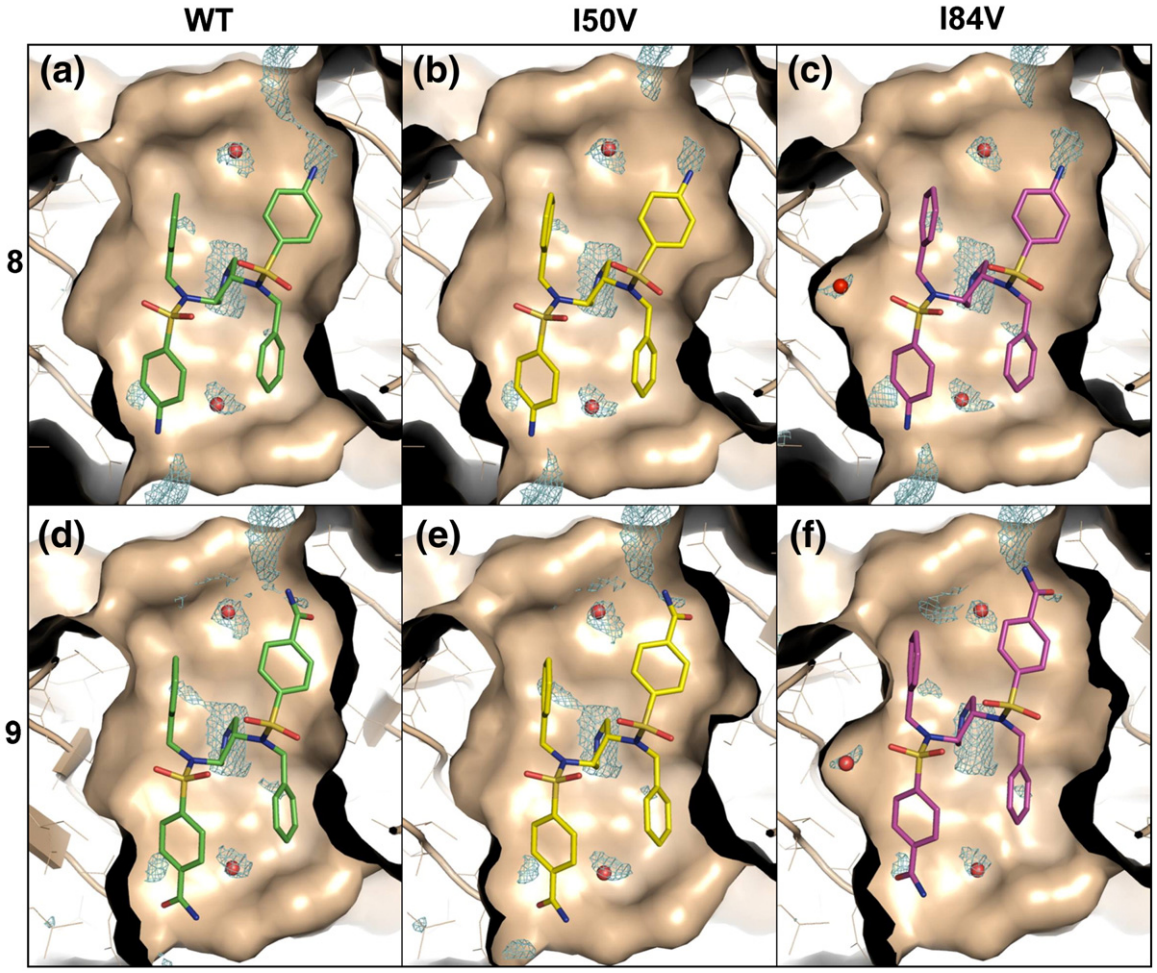

Fig. 6. The calculated GRID interaction fields for the binding pockets of PR_{WT} (a and d), PR_{I50V} (b and e), and PR_{I84V} (c and f) in complex with compounds **8** (a–c) and **9** (d–f) are displayed as blue mesh at a contour level of 8 kcal/mol. The protein surface is schematically represented in wheat, and the corresponding ligand is color coded by atom type in green, yellow, and magenta for PR_{WT}, PR_{I50V}, and PR_{I84V}, respectively. Experimental observed water molecules are shown as red spheres.

Energetically favorable water contacts are predicted in the region surrounding the catalytic Asp25A and Asp25B, at the far end of the S2 and S2′ pockets and next to Gly27A and Gly27B. The position of the additionally enclosed water molecule is identified as preferred position for a water molecule only in the case of PR_{I84V} (Fig. 6d and e). The positions of the experimentally observed waters are in good agreement with the calculated interaction fields.

Table 5. Polar contacts of ligand **9** observed in the co-crystal structures with the different HIV protease variants

	PR_{WT} (Å)	PR_{I50V} (Å)	PR_{I84V} (Å)
D25 O^{δ}	2.7–3.0	2.7–3.0	2.7–2.9
I/V50A N	3.0	3.0	3.2
I/V50B N	3.2	3.5	3.6
D29A O^{δ}/H_2O	3.0/2.7	3.4/2.5	3.1/2.4
D30A N	3.0	3.0	3.0
D30B O^{δ}	2.9	2.9	3.1
D30B N	2.8	3.0	2.9

Discussion

The intention of this study was to elucidate the potential of a new class of HIV PIs against crucial point mutations. The unique mode in addressing the enzyme's subpockets observed for the C_2-symmetric pyrrolidines suggests deviating susceptibility towards amino acid exchanges at the S1/S2′ and S1′/S2 pocket interfaces. The studied variants Ile50Val and Ile84Val are major mutations, both expanding the protease's binding pocket. Kinetic characterization reveals significant affinity decrease towards all four applied fluorogenic substrates with respect to the mutants. Similar observations are made for the inhibitors in the case of the Ile50Val mutation; however, they were less pronounced as compared to the substrates. In contrast, the inhibitors retain or even increase affinity towards the Ile84Val mutant. Obviously, removal of the methylene groups results in a different response in terms of binding affinity.

Both inhibitors **8** and **9** are almost completely buried in all complexes due to the tunnel-shaped

binding cavity of the protease. The mutations at the pivotal positions do not influence the burial of the ligands.

With respect to the Ile50Val complexes, a high level of similarity with the wild-type counterparts is observed. The side chains of Ile50B form presumably unfavorable close contacts to the sulfonyl oxygen atoms in PR_{WT} and PR_{I50V}. In the wild-type protease, C^{δ} of Ile50A is in van der Waals contact to carbon atoms of the phenyl moiety of compounds **8** and **9**. In contrast, in PR_{I50V}, the isoleucine exchange results in a loss of these favorable interactions, thus explaining the drop in inhibitor affinity. In the case of amprenavir, which bears a similar P2′ moiety, the susceptibility towards the Ile50Val mutation is also attributed to these interactions.[26]

Larger differences are observed in the case of the PR_{I84V} complexes. Ligand and protein conformation, along with the formed polar interactions, is highly conserved. In PR_{I84V}, C^{δ} of Ile50B forms van der Waals contacts to the phenyl moiety of the inhibitors. This contact is not observed in the wild type. Regarding the PR_{WT} complexes, the C^{δ} atoms of Ile84A and Ile84B have unfavorable short van der Waals contacts with ligand atoms. Through exchange of these residues to valine, these unfavorable contacts are relaxed. The overall hydrophobic surface present in PR_{WT} and PR_{I50V} changes significantly, leading to a stronger exposure of the polar surfaces of Thr80 and Val82. In the wild-type complexes, the hydroxyl group of Thr80 is generally involved in a hydrogen bond to the main-chain carbonyl of Val82. As a result of the created additional space in PR_{I84V}, a water molecule is picked up and participates in polar interactions, forming a hydrogen-bond network connecting Thr80A and Val82A with one sulfonyl oxygen atom of the ligand. In PR_{WT} complexes, this oxygen atom is not involved in any polar interactions. At the symmetry-related B-domain, intercalation of a water molecule is not observed in the mutant, likely due to the shorter distance of the sulfonyl oxygen atom to the polar groups. Considering the results of a GRID analysis, the intercalation of a water molecule seems to be highly favorable in the A-domain. The additional hydrogen bonds to Thr80A and Val82A and the loss of short van der Waals contacts to the residue in position 84A induce a slightly different loop conformation of the A-chain residues 79–84 of PR_{I84V}. This is reflected by an increased rmsd of this region to PR_{WT}: 0.56 Å in the case of compound **8** and 0.54 Å in the case of compound **9**. This reorganization leads to a better mutual surface match of the ligand in the S1 pocket. In summary, these contributions add up to an improved affinity of this class of ligands towards the Ile84Val mutant. The amount of each individual contribution is difficult to assign and will depend on slight differences in the shape and accordingly accommodated binding mode. Clearly, the individual contributions are not additive as can be seen when compounds **8**, **9** and **10** are compared. Inhibitors **8** *versus* **9** and **10** are equipped with different polar substituents (NH_2 *versus* $CONH_2$). They induce slightly different arrangements in the corresponding S2/S2′ pockets. Via the rigid central scaffold, this discrepancy is translated into small orientational differences of the ligands in the S1/S1′ pockets. They result in shorter van der Waals contacts to Ile84 for compound **9** compared to compound **8**. Mutating this residue to the smaller valine results in a relief of steric strain and provokes the observed increase in affinity discrimination between PR_{I84V} and PR_{WT}.

Summary and Conclusion

The investigated pyrrolidine-based inhibitors provide a novel strategy to target the subpockets of HIV protease. This leads to a different occupation of the binding pocket, especially next to the border between the S1/S2′ and S1′/S2 pockets. The properties of the new inhibitor class have been examined towards the active-site mutations Ile50Val and Ile84Val. Kinetic data indicate a contrary behavior: reduced affinity towards PR_{I50V} and improved potency towards PR_{I84V}. The determination of co-crystal structures of two representative inhibitors (compounds **8** and **9**) with the wild type and the two variants provides the structural basis to explain this observation. The reduced affinity towards PR_{I50V} could be rationalized in terms of reduced van der Waals contacts, an observation already described in literature for amprenavir. In the case of PR_{I84V}, multiple contributions are responsible: Amplified van der Waals contacts, enhanced polar interactions mediated by an intercalating water molecule that fills the gap created by the mutational exchange, and relief of steric strain likely given in the wild-type complexes. The Ile84Val mutation is discussed in literature mainly as an expansion of the active-site volume, lowering beneficial van der Waals contacts to a bound ligand. Here, we can trace the exchange in more detail and make changes in the exposed physicochemical properties responsible for the modified interaction profile. The investigated pyrrolidines are very rigid ligands. They cannot optimally adapt their shape to the PR_{WT} binding pocket. Surface complementarity of the PR_{I84V} binding pocket is more appropriate to accommodate an inhibitor compared to the wild type, exhibiting, in best case, a K_i of 12 nM for compound **10**.

The message to be learned from this study concerns the change in physicochemical properties of the binding pocket upon Ile84Val mutation that can be exploited for inhibitor design. Taking advantage of these features might avoid the susceptibility towards this mutation, which has proven to be problematic for all presently approved inhibitors.

Furthermore, this study unambiguously shows that large affinity changes, for example, a factor of 40 in the case of compound **9**, might result from very small deviations in the protein–ligand complexes. It also points to the limitations in modeling such differences. Only the detailed analysis of multiple complexes in terms of structure–activity relationships provides

deeper insights into the various contributions responsible for protein–ligand interactions.

Experimental Procedures

Inhibitor preparation

The inhibitors were synthesized enantioselectively from D-(−)-tartaric acid as recently reported.[12] Stock solutions of inhibitors for kinetic measurements and co-crystallization were obtained by dissolving them in dimethyl sulfoxide (DMSO).

Mutant preparation, purification, and crystallization

Mutants were prepared using the polymerase chain reaction with the QuikChange Site-Directed Mutagenesis Kit (Stratagene).[29] The pET11a plasmid containing the HIV-1 protease gene was kindly provided by Professor Helena Danielson, University of Uppsala. Synthetic oligonucleotides containing the desired mutation were used as mutagenic primers: 5′-CCAAAAATGATAGGGGGAGTTGGAGGTTTTATCAAAGTAAG-3′ and 5′-CTTACTTTGATAAAACCTCCAACTCCCCCTATCATTTTGG-3′ for I50V and 5′-GGACCTACACCTGTCAACGTAATTGGAAGAAATCTGTTG-3′ and 5′-CAACAGATTTCTTCCAATTACGTTGACAGGTGTAGGTCC-3′ for I84V. All constructs were verified by DNA sequencing. The PR_{WT}, PR_{I50V}, and PR_{I84V} HIV protease variants were consecutively expressed from *Escherichia coli* and purified as previously described.[30]

The HIV PI complexes were crystallized at 18 °C by the sitting drop vapor diffusion method using a 1:1 ratio. Crystals were obtained by co-crystallization of the enzyme with inhibitor concentrations ranging from 50- to 100-fold the K_i value and a final DMSO concentration of 5%. One microliter of the well buffer (0.1 M Bis–Tris and 2.5–3.0 M NaCl, pH 6.5) was mixed with 1 μL of the protein solution (50 mM NaOAc, 1 mM ethylenediaminetetraacetic acid, and 1 mM DTT, pH 6.5) with an HIV protease concentration of 7–10 mg/mL. Crystals were obtained within 1–2 days and exhibited a rectangular shape. Crystals were further optimized using streak-seeding techniques. For cryoprotection, the crystals were briefly soaked in mother liquor containing 25% glycerol.

Kinetic assay

Enzymatic assays were performed in 172 μL assay buffer (100 mM 4-morpholineethanesulfonic acid, 300 mM KCl, 5 mM ethylenediaminetetraacetic acid, and 1 mg/mL bovine serum albumin, pH 5.5) by the addition of substrate dissolved in 4 μL DMSO, distinct inhibitor concentrations dissolved in 4 μL DMSO, and 20 μL HIV-1 protease in assay buffer to a final volume of 200 μL (final DMSO concentration, 4%). Fluorogenic anthranilyl-HIV protease substrates A [Abz-Thr-Ile-Nle-(*p*-NO_2-Phe)-Gln-Arg-NH_2] and B [Abz-Lys-Ala-Arg-Val-Nle-(*p*-NO_2-Phe)-Phe-Glu-Ala-Nle-NH_2] were purchased from Bachem, and substrates C [Abz-Ala-Arg-Val-Nle-(*p*-NO_2-Phe)-Phe-Glu-Ala-Nle-NH_2] and D [Abz-Arg-Val-Nle-(*p*-NO_2-Phe)-Phe-Glu-Ala-Nle-NH_2] were from Sigma-Aldrich. The kinetic constants for PR_{WT}, PR_{I50V}, and PR_{I84V} were determined by the method of Lineweaver and Burk. The total enzyme concentration was quantified by titrating with the strong binding inhibitor saquinavir at a 200-fold higher enzyme concentration. Inhibition data for PR_{WT}, PR_{I50V}, and PR_{I84V} were determined as follows: IC_{50} values were taken from plots of v_i/v_0 *versus* inhibitor concentration, in which v_i and v_0 are the velocities in the presence and in the absence of an inhibitor, respectively. The hydrolysis of substrate A was recorded as the increase in fluorescence intensity (excitation wavelength, 337 nm; emission wavelength, 410 nm) over a time period of 10 min, during which the signal increased linearly with time.[31] K_i values were calculated from the following equation: $K_i = [IC_{50} - (E_t/2)][1 + (S/K_m)]^{-1}$.

Data collection, phasing, and refinement

The data sets were collected at the synchrotron BESSY II in Berlin/Germany on PSF beamline 14.2 (**8** PR_{I50V}, PDB ID: 2R43), equipped with a MAR-CCD detector, and on a Rigaku R-AXIS IV image plate detector using Cu K_α radiation from an in-house Rigaku rotating anode (**8** PR_{I84V}, PDB ID: 2R3W; **9** PR_{I50V}, PDB ID: 2R3T; and **9** PR_{I84V}, PDB ID: 2R38). Data were processed and scaled with Denzo and Scalepack as implemented in HKL2000.[32] The structures were determined by the molecular replacement method with Phaser;[33] one monomer of the 1.50-Å HIV-1 protease in complex with a pyrrolidine-based inhibitor (PDB ID: 2PQZ) was used as the search model. The structure refinement was continued with SHELXL-97;[34] for each refinement step, at least 10 cycles of conjugate gradient minimization were performed, with restraints on bond distances, angles, and *B*-values. Intermittent cycles of model building were done with the program Coot.[35]

GRID analysis and surface calculations

The calculations of the molecular interaction fields were performed with GREATER, a graphical user interface for the program GRID, version 22.[36] The interaction box was defined to enclose the entire active sites. The grid spacing was equal to 0.33 Å (NPLA = 3), and the maximum positive cutoff energy was set to 8 kcal/mol and visualized with PyMOL.[37] The buried surface area was calculated with the program MS developed by Connolly.[38] The program calculates the molecular surface from atom coordinates; the probe radius was set to 1.4 Å.

PDB accession numbers

Coordinates and structure factors have been deposited in the PDB‡ with accession numbers 2R43 (**8** PR_{I50V}), 2R3W (**8** PR_{I84V}), 2R3T (**9** PR_{I50V}), and 2R38 (**9** PR_{I84V}).

Acknowledgements

We acknowledge the support of the beamline staff at BESSY II, Berlin, Germany, and thank the Bundesministerium für Bildung und Forschung (05 ES3XBA/5) for financing the travel costs to BESSY II. The pET11a plasmid containing the HIV-1 protease gene was kindly provided by Professor

‡ http://www.rcsb.org/pdb/

Helena Danielson, University of Uppsala, Sweden. This work was also supported by a fellowship (A.B.) from the Fonds der Chemischen Industrie.

References

1. Wlodawer, A. & Erickson, J. W. (1993). Structure-based inhibitors of HIV-1 protease. *Annu. Rev. Biochem.* **62**, 543–585.
2. Kramer, R. A., Schaber, M. D., Skalka, A. M., Ganguly, K., Wong-Staal, F. & Reddy, E. P. (1986). HTLV-III gag protein is processed in yeast cells by the virus pol-protease. *Science*, **231**, 1580–1584.
3. Kohl, N. E., Emini, E. A., Schleif, W. A., Davis, L. J., Heimbach, J. C., Dixon, R. A. F. *et al.* (1988). Active human immunodeficiency virus protease is required for viral infectivity. *Proc. Natl Acad. Sci. USA*, **85**, 4686–4690.
4. Flexner, C. (2007). HIV drug development: the next 25 years. *Nat. Rev., Drug Discov.* **6**, 959–966.
5. Bartlett, J. A., DeMasi, R., Quinn, J., Moxham, C. & Rousseau, F. (2001). Overview of the effectiveness of triple combination therapy in antiretroviral-naive HIV-1 infected adults. *AIDS*, **15**, 1369–1377.
6. Gulick, R. M., Mellors, J. W., Havlir, D., Eron, J. J., Meibohm, A., Condra, J. H. *et al.* (2000). 3-year suppression of HIV viremia with indinavir, zidovudine, and lamivudine. *Ann. Intern. Med.* **133**, 35–39.
7. Coffin, J. M. (1995). HIV population dynamics *in vivo*: implications for genetic variation, pathogenesis, and therapy. *Science*, **267**, 483–489.
8. Mendoza, C. d. & Vincent, S. (2004). Resistance to HIV protease inhibitors: mechanisms and clinical consequences. *Curr. Drug Metab.* **5**, 321–328.
9. Ohtaka, H., Muzammil, S., Schön, A., Velazquez-Campoy, A., Vega, S. & Freire, E. (2004). Thermodynamic rules for the design of high affinity HIV-1 protease inhibitors with adaptability to mutations and high selectivity towards unwanted targets. *Int. J. Biochem. Cell Biol.* **36**, 1787–1799.
10. D'Aquila, R. T., Schapiro, J. M., Brun-Vézinet, F., Clotet, B., Conway, B., Demeter, L. M. *et al.* (2002). Drug resistance mutations in HIV-1. *Top. HIV Med.* **10**, 21–25.
11. Specker, E., Böttcher, J., Lilie, H., Heine, A., Schoop, A., Müller, G. *et al.* (2005). An old target revisited: two new privileged skeletons and an unexpected binding mode for HIV-protease inhibitors. *Angew. Chem., Int. Ed.* **44**, 3140–3144.
12. Blum, A., Böttcher, J., Heine, A., Klebe, G. & Diederich, W. E. (2008). Structure guided design of C_2-symmetric HIV-1 protease inhibitors based on a pyrrolidine scaffold. *J. Med. Chem.* **51**, 2078–2087.
13. Kempf, D. J., Marsh, K. C., Denissen, J. F., McDonald, E., Vasavanonda, S., Flentge, C. A. *et al.* (1995). ABT-538 is a potent inhibitor of human immunodeficiency virus protease and has high oral bioavailability in Humans. *Proc. Natl Acad. Sci. USA*, **92**, 2484–2488.
14. Clemente, J. C., Coman, R. M., Thiaville, M. M., Janka, L. K., Jeung, J. A., Nukoolkarn, S. *et al.* (2006). Analysis of HIV-1 CRF_01 A/E protease inhibitor resistance: structural determinants for maintaining sensitivity and developing resistance to atazanavir. *Biochemistry*, **45**, 5468–5477.
15. Surleraux, D. L. N. G., Tahri, A., Verschueren, W. G., Pille, G. M. E., de Kock, H. A., Jonckers, T. H. M. *et al.* (2005). Discovery and selection of TMC114, a next generation HIV-1 protease inhibitor. *J. Med. Chem.* **48**, 1813–1822.
16. Kim, E. E., Baker, C. T., Dwyer, M. D., Murcko, M. A., Rao, B. G., Tung, R. D. & Navia, M. A. (1995). Crystal structure of HIV-1 protease in complex with VX-478, a potent and orally bioavailable inhibitor of the enzyme. *J. Am. Chem. Soc.* **117**, 1181–1182.
17. Chen, Z., Li, Y., Chen, E., Hall, D. L., Darke, P. L., Culberson, C. *et al.* (1994). Crystal structure at 1.9-Å resolution of human immunodeficiency virus (HIV) II protease complexed with L-735,524, an orally bioavailable inhibitor of the HIV proteases. *J. Biol. Chem.* **269**, 26344–26348.
18. Kaldor, S. W., Kalish, V. J., Davies, J. F., Shetty, B. V., Fritz, J. E., Appelt, K. *et al.* (1997). Viracept (nelfinavir mesylate, AG1343): a potent, orally bioavailable inhibitor of HIV-1 protease. *J. Med. Chem.* **40**, 3979–3985.
19. Krohn, A., Redshaw, S., Ritchie, J. C., Graves, B. J. & Hatada, M. H. (1991). Novel binding mode of highly potent HIV-proteinase inhibitors incorporating the (*R*)-hydroxyethylamine isostere. *J. Med. Chem.* **34**, 3340–3342.
20. Muzammil, S., Armstrong, A. A., Kang, L. W., Jakalian, A., Bonneau, P. R., Schmelmer, V. *et al.* (2007). Unique thermodynamic response of tipranavir to human immunodeficiency virus type 1 protease drug resistance mutations. *J. Virol.* **81**, 5144–5154.
21. Tisdale, M., Myers, R., Randall, S., Maguire, M., Ait-Khaled, M., Elston, R. & Snowden, W. (2000). Resistance to the HIV protease inhibitor amprenavir *in vitro* and in clinical studies: a review. *Clin. Drug Invest.* **20**, 267–285.
22. Pazhanisamy, S., Stuver, C. M., Cullinan, A. B., Margolin, N., Rao, B. G. & Livingston, D. J. (1996). Kinetic characterization of human immunodeficiency virus type-1 protease-resistant variants. *J. Biol. Chem.* **271**, 17979–17985.
23. Klabe, R. M., Bacheler, L. T., Ala, P. J., Erickson-Viitanen, S. & Meek, J. L. (1998). Resistance to HIV protease inhibitors: a comparison of enzyme inhibition and antiviral potency. *Biochemistry*, **37**, 8735–8742.
24. Tie, Y., Kovalevsky, A. Y., Boross, P., Wang, Y., Ghosh, A. K., Tozser, J. *et al.* (2007). Atomic resolution crystal structures of HIV-1 protease and mutants V82A and I84V with saquinavir. *Proteins*, **67**, 232–242.
25. Wang, Y., Tie, Y., Boross, P. I., Tozser, J., Ghosh, A. K., Harrison, R. W. & Weber, I. T. (2007). Potent new antiviral compound shows similar inhibition and structural interactions with drug resistant mutants and wild type HIV-1 protease. *J. Med. Chem.* **50**, 4509–4515.
26. Ohtaka, H., Velázquez-Campoy, A., Xie, D. & Freire, E. (2002). Overcoming drug resistance in HIV-1 chemotherapy: the binding thermodynamics of amprenavir and TMC-126 to wild-type and drug-resistant mutants of the HIV-1 protease. *Protein Sci.* **11**, 1908–1916.
27. Todd, M. J., Luque, I., Velázquez-Campoy, A. & Freire, E. (2000). Thermodynamic basis of resistance to HIV-1 protease inhibition: calorimetric analysis of the V82F/I84V active site resistant mutant. *Biochemistry*, **39**, 11876–11883.
28. Wang, W. & Kollman, P. A. (2001). Computational study of protein specificity: the molecular basis of HIV-1 protease drug resistance. *Proc. Natl. Acad. Sci. USA*, **98**, 14937–14942.
29. Saiki, R. K., Gelfand, D. H., Stoffel, S., Scharf, S. J., Higuchi, R., Horn, G. T. *et al.* (1988). Primer-directed enzymatic amplification of DNA with a thermostable DNA polymerase. *Science*, **239**, 487–491.

30. Taylor, A., Brown, D. P., Kadam, S., Maus, M., Kohlbrenner, W. E., Weigl, D. *et al.* (1992). High-level expression and purification of mature HIV-1 protease in *Escherichia coli* under control of the araBAD promoter. *Appl. Microbiol. Biotechnol.* **37**, 205–210.
31. Toth, M. V. & Marshall, G. R. (1990). A simple, continuous fluorometric assay for HIV protease. *Int. J. Pept. Protein Res.* **36**, 544–550.
32. Otwinowski, Z. & Minor, W. (1997). Processing of X-ray diffraction data collected in oscillation mode. In *Methods in Enzymology* (Carter, C. W., Jr & Sweet, R. M., eds), Vol. 276, pp. 307–326. Academic Press, San Diego, London.
33. Storoni, L. C., McCoy, A. J. & Read, R. J. (2004). Likelihood-enhanced fast rotation functions. *Acta Crystallogr., Sect. D: Biol. Crystallogr.* **60**, 432–438.
34. Sheldrick, G. M. & Schneider, T. R. (1997). SHELXL: high-resolution refinement. In *Methods in Enzymology* (Carter, C. W., Jr & Sweet, R. M., eds), Vol. 277, pp. 319–343. Academic Press, San Diego, London.
35. Emsley, P. & Cowtan, K. (2004). Coot: model-building tools for molecular graphics. *Acta Crystallogr., Sect. D: Biol. Crystallogr.* **60**, 2126–2132.
36. Goodford, P. J. (1985). A computational procedure for determining energetically favorable binding sites on biologically important macromolecules. *J. Med. Chem.* **28**, 849–857.
37. DeLano, W. L. (2002). *The PyMOL Molecular Graphics System.* DeLano Scientific, San Carlos, CA; http://pymol.sourceforge.net/
38. Connolly, M. L. (1983). Analytical molecular surface calculation. *J. Appl. Crystallogr.* **16**, 548–558.